

See discussions, stats, and author profiles for this publication at: <https://www.researchgate.net/publication/228771700>

Modelling of Fluid-Conveying Flexible Pipes in Multibody Systems

Article · October 2009

CITATIONS

2

READS

219

2 authors, including:



[W.B.J. Hakvoort](#)

University of Twente

27 PUBLICATIONS 146 CITATIONS

[SEE PROFILE](#)

Some of the authors of this publication are also working on these related projects:



Active vibration isolation control for Coriolis Flow Meters [View project](#)

MODELLING OF FLUID-CONVEYING FLEXIBLE PIPES IN MULTIBODY SYSTEMS

J. P. Meijaard¹ and W. B. J. Hakvoort^{1,2}

¹Laboratory of Mechanical Automation and Mechatronics, CTW/WA, University of Twente,
P.O. Box 217, NL-7500 AE Enschede, The Netherlands
e-mail: {J.P.Meijaard,W.B.J.Hakvoort}@utwente.nl

²Demcon
Oldenzaal, The Netherlands

Keywords: Flexible Multibody Dynamics, Fluid-Conveying Pipes, Curved Beam Element, Stability, Coriolis Mass-Flow Rate Meter.

Abstract. *The modelling and simulation of flexible multibody systems containing fluid-conveying pipes are considered. The mass-flow rate is assumed to be prescribed and constant and the pipe cross-section is piecewise uniform. An existing beam element is modified to include the effect of the fluid flow and the initial curvature of the pipe. The element is applied in several test problems: the buckling of a simply supported pipe, the flutter instability of a cantilever pipe and the motion of a curved pipe that can rotate about an axis perpendicular to its plane. As a three-dimensional example, a Coriolis mass-flow rate meter with a U-shaped pipe is considered.*

1 INTRODUCTION

The dynamics of pipes conveying fluids has been the subject of a considerable amount of research. Païdoussis [1] presents and discusses the most important contributions. Instabilities, both of the divergent and flutter type, and non-linear phenomena after the instability has occurred have been studied. Benjamin [2, 3] studied the dynamics of articulated pipes both theoretically and experimentally. The equations of motion were derived with a modification of Lagrange's equations for open systems, which has more recently been generalized [4]. The corresponding case for a continuous cantilever beam was subsequently analysed [5, 6]. An example of the study of non-linear oscillations is [7]. Numerical modelling of the dynamics by finite elements has been done repeatedly, but the integration with flexible multibody systems for simulating pipes that can undergo arbitrarily large overall motions, however, is still largely an open field. A formulation for the planar case has been presented in [8].

The advantages of having available fluid-conveying pipes as modelling elements in a multibody dynamics system is that the interaction with other parts of a mechanical system can be modelled in a single system and all analysis tools for these systems are readily available, such as linearization and the combination with measurement and control systems. The direct incentive to the present study was the demand to model Coriolis mass-flow rate meters, in which a flexible fluid-conveying pipe is excited in a particular eigenmode for the system with stationary fluid and measurements are made on another mode, which is excited by the Coriolis term due to the fluid flow in the equations of motion, from which the mass-flow rate can be deduced [9, 10]. Even if the shape of the pipe is planar, the motion is in most designs predominantly out of its plane and a three-dimensional model is needed.

In this paper, a finite element to model fluid-conveying pipes that can undergo arbitrarily large motions and may suffer deformations is developed. It is basically a modification of a two-node curved beam element to which the influence of an internal mass flow is added. The element is applied to some test problems, viz the buckling of a simply supported pipe by the fluid flow, the flutter instability of a cantilever pipe with free outflow and the acceleration of a semicircular pipe that can rotate about its inlet point, as in garden sprinkler, up to its stationary speed. As a final application, the dynamics of a Coriolis mass-flow rate meter are analysed and results are compared with those of another program and with theoretical and experimental results from the literature.

2 PIPE ELEMENT

The pipe element developed here is a modification of an existing two-node beam element [11] that includes the effects of the internal flow. Its nodal coordinates are the position and the orientation parameters of the end-nodes, which describe the positions and orientations of the two planes of the cross-section at the ends of a part of a pipe. Global Cartesian coordinates are used for the positions and Euler parameters for the orientations, but this is not essential for the formulation. Furthermore, the total mass of the fluid that has passed the cross-section at a node starting from some initial time is a nodal coordinate. The time derivatives of these masses are the mass-flow rates through the nodal cross-sections. The pipe element can be initially curved in space.

2.1 Generalized strains

The free element has 14 independent nodal coordinates. Besides the six customary rigid-body degrees of freedom, the element has an additional rigid-body displacement, which is char-

acterized by a constant mass flow over the length of the element. Therefore, seven independent generalized strains can be defined which are required to be invariant for arbitrary rigid-body displacements; assigning prescribed values to these generalized strains imposes the conditions of rigidity of the element, whereas all arbitrarily large rigid-body displacements are unrestrained.

The position vectors at the nodes p and q are denoted by \mathbf{x}^p and \mathbf{x}^q , respectively. These are attached to the elastic centres of the cross-sections. The orientations of the nodes are given by orthogonal triads of unit vectors, $\mathbf{e}_x^p, \mathbf{e}_y^p, \mathbf{e}_z^p$ at node p and $\mathbf{e}_x^q, \mathbf{e}_y^q, \mathbf{e}_z^q$, at node q . The unit vectors $\mathbf{e}_x^{p,q}$ are perpendicular to the cross-sections, at node p pointing into the element and at node q pointing outwards, and the other two are in the cross-sections in the principal directions. The parameters to describe the orientations are denoted by $\boldsymbol{\vartheta}^p$ for node p and $\boldsymbol{\vartheta}^q$ for node q .

The six generalized strains of the beam are given by [11]

$$\begin{aligned}\varepsilon_1 &= \bar{\varepsilon}_1 + (2\bar{\varepsilon}_3^2 + \bar{\varepsilon}_3\bar{\varepsilon}_4 + 2\bar{\varepsilon}_4^2 + 2\bar{\varepsilon}_5^2 + \bar{\varepsilon}_5\bar{\varepsilon}_6 + 2\bar{\varepsilon}_6^2)/(30l_0), \\ \varepsilon_2 &= \bar{\varepsilon}_2 + (-\bar{\varepsilon}_3\bar{\varepsilon}_6 + \bar{\varepsilon}_4\bar{\varepsilon}_5)/l_0, \\ \varepsilon_3 &= \bar{\varepsilon}_3 + \bar{\varepsilon}_2(\bar{\varepsilon}_5 + \bar{\varepsilon}_6)/(6l_0), \\ \varepsilon_4 &= \bar{\varepsilon}_4 - \bar{\varepsilon}_2(\bar{\varepsilon}_5 + \bar{\varepsilon}_6)/(6l_0), \\ \varepsilon_5 &= \bar{\varepsilon}_5 - \bar{\varepsilon}_2(\bar{\varepsilon}_3 + \bar{\varepsilon}_4)/(6l_0), \\ \varepsilon_6 &= \bar{\varepsilon}_6 + \bar{\varepsilon}_2(\bar{\varepsilon}_3 + \bar{\varepsilon}_4)/(6l_0),\end{aligned}\tag{1}$$

where l_0 is the reference length of the beam. The barred quantities are given by

$$\begin{aligned}\bar{\varepsilon}_1 &= l - l_0, \\ \bar{\varepsilon}_2 &= l_0(\mathbf{e}_z^p \cdot \mathbf{e}_y^q - \mathbf{e}_y^p \cdot \mathbf{e}_z^q)/2, \\ \bar{\varepsilon}_3 &= -l_0\mathbf{e}_l \cdot \mathbf{e}_z^p, \\ \bar{\varepsilon}_4 &= l_0\mathbf{e}_l \cdot \mathbf{e}_z^q, \\ \bar{\varepsilon}_5 &= l_0\mathbf{e}_l \cdot \mathbf{e}_y^p, \\ \bar{\varepsilon}_6 &= -l_0\mathbf{e}_l \cdot \mathbf{e}_y^q,\end{aligned}\tag{2}$$

where $l = \|\mathbf{x}^q - \mathbf{x}^p\|$ is the actual distance between the nodes and $\mathbf{e}_l = (\mathbf{x}^q - \mathbf{x}^p)/l$ is a unit vector pointing from the current position of node p to the current position of node q .

The seventh generalized strain is chosen as proportional to the increase in fluid mass between the two cross-sections at the nodes, so it is the difference between the two nodal fluid mass flows, scaled with the reference mass per unit of length,

$$\varepsilon_7 = \frac{m^p - m^q}{\rho_{f0}A_f},\tag{3}$$

where ρ_{f0} is the reference mass density of the fluid and A_f is the reference enclosed surface of the cross-section. The scaling results in generalized strains having length as their physical dimension.

The energetic duals of the generalized strains are the generalized stresses, such that $-\boldsymbol{\sigma}^T \delta \boldsymbol{\varepsilon}$ represents the virtual work of the stress resultants, where the seven generalized strains have been grouped into a column vector $\boldsymbol{\varepsilon}$ and likewise the seven generalized stresses into a column vector $\boldsymbol{\sigma}$. A virtual variation is denoted by a prefixed δ . The meaning of the generalized stresses can be found from the equilibrium conditions

$$\delta \mathbf{u}^T \mathbf{f} - \delta \boldsymbol{\varepsilon}^T \boldsymbol{\sigma} = \delta \mathbf{u}^T (\mathbf{f} - \mathbf{D}^T \boldsymbol{\sigma}) = 0,\tag{4}$$

where \mathbf{f} are the nodal forces dual to the virtual nodal displacements $\delta\mathbf{u}$, which comprise all contributions including inertial terms. The difference matrix \mathbf{D} represents the relations between virtual nodal point displacements and virtual strains, $\delta\varepsilon = \mathbf{D}\delta\mathbf{u}$, which follow from Eqs. (1–3) by taking derivatives. From Eq. (4) follow the equilibrium equations

$$\mathbf{f} - \mathbf{D}^T \boldsymbol{\sigma} = \mathbf{0}. \quad (5)$$

The rows of \mathbf{D} represent the nodal force systems that give rise to the individual components of the generalized stresses. For small strains, one can observe that σ_1 represents the total normal force in the element, including the contribution of the pressure in the fluid, σ_2 is the torsional moment divided by the beam length, σ_3 , σ_4 , σ_5 and σ_6 are the bending moments, divided by the beam length, at the nodes in the principal directions and σ_7 is the compressive force in the fluid, that is, the pressure times the cross-section of the fluid, at the nodes.

The constitutive equations for bending and torsion are assumed not to be influenced by the internal pressure in the pipe and are taken the same as for the original beam element,

$$\begin{aligned} \sigma_2 &= \frac{k_x G I_p}{l_0^3} (\varepsilon_2 - \varepsilon_{02}), \\ \begin{bmatrix} \sigma_3 \\ \sigma_4 \end{bmatrix} &= \frac{E I_y}{(1 + \Phi_z) l_0^3} \begin{bmatrix} 4 + \Phi_z & -2 + \Phi_z \\ -2 + \Phi_z & 4 + \Phi_z \end{bmatrix} \begin{bmatrix} \varepsilon_3 - \varepsilon_{03} \\ \varepsilon_4 - \varepsilon_{04} \end{bmatrix}, \\ \begin{bmatrix} \sigma_5 \\ \sigma_6 \end{bmatrix} &= \frac{E I_z}{(1 + \Phi_y) l_0^3} \begin{bmatrix} 4 + \Phi_y & -2 + \Phi_y \\ -2 + \Phi_y & 4 + \Phi_y \end{bmatrix} \begin{bmatrix} \varepsilon_5 - \varepsilon_{05} \\ \varepsilon_6 - \varepsilon_{06} \end{bmatrix}. \end{aligned} \quad (6)$$

Here, E is the modulus of elasticity of the pipe material, G is its shear modulus, I_y and I_z are the area moments of inertia of the cross-section of the pipe about the local y - and z -axis, respectively, $I_p = I_y + I_z$ is the polar moment of inertia and k_x is a shape factor for non-circular cross-sections. ε_{02} to ε_{06} are the values of the generalized strains for which the beam is stress-free. The transverse shear deflection is taken into account with the factors

$$\Phi_z = \frac{12 E I_y}{G A_p k_z l_0^2}, \quad \Phi_y = \frac{12 E I_z}{G A_p k_y l_0^2}, \quad (7)$$

where A_p is the area of the pipe cross-section and k_y and k_z are transverse shear coefficients in the y - and z -direction, respectively.

For a thin-walled tube with circular cross-section with radius r and wall thickness t , the relations between ε_1 , ε_7 , σ_1 and σ_7 are

$$\begin{bmatrix} \varepsilon_1 \\ \varepsilon_7 \end{bmatrix} = \frac{l_0}{E A_p} \begin{bmatrix} 1 & 1 - 2\nu \\ 1 - 2\nu & 5 - 4\nu + 2Et/(Kr) \end{bmatrix} \begin{bmatrix} \sigma_1 \\ \sigma_7 \end{bmatrix}, \quad (8)$$

where K is the bulk modulus of the fluid and $\nu = E/(2G) - 1$ is Poisson's ratio of the pipe material. This relation can be obtained from considering a pipe loaded with a tensile force $\sigma_1 + \sigma_7$ and a compressive force σ_7 on the fluid. Similar relations hold for thick-walled pipes and pipes with a non-circular cross-section. An initial elongation can be taken into account by modifying l_0 . Fluid friction can be included as generalized forces acting on the nodal variables m^p and m^q .

The element can be simplified if it is assumed that there is no accumulation of fluid in the element and the mass-flow rate is a prescribed function of time. We then clearly have $\varepsilon_7 = 0$ and σ_7 appears as a Lagrangian multiplier, which is not included in the analysis, since the

constraint is satisfied by prescribing equal mass flows at both nodes. So the element has the same number of nodal coordinates and generalized strains as the spatial beam element. A further simplification occurs if the axial strain, ε_1 , is neglected and the mass-flow rate is assumed to be constant.

2.2 Inertial effects

With the curve length s along the axis of the pipe in its reference position, measured from node p towards node q , $0 \leq s \leq l_0$, the position of a material cross-section at $s = l_0\xi$ of the pipe can be approximated as

$$\mathbf{x}(\xi) = \mathbf{x}^p(1 - 3\xi^2 + 2\xi^3) + l_0\mathbf{e}_x^p(\xi - 2\xi^2 + \xi^3) + \mathbf{x}^q(3\xi^2 - 2\xi^3) + l_0\mathbf{e}_x^q(-\xi^2 + \xi^3). \quad (9)$$

This interpolation is chosen independently from the deflection of the pipe, and so only approximates it. Only the translation component is taken into account in a distributed way; the mass moments of inertia of the cross-sections are lumped to the adjacent nodes. The resulting mass formulation is therefore not fully consistent. The velocity and acceleration can be obtained from this expression by differentiations. The virtual work due to the inertia terms is

$$-\rho_p A_p l_0 \int_0^1 \delta \mathbf{x}^T \ddot{\mathbf{x}} d\xi = -\delta \mathbf{x}^{eT} [\mathbf{M}_{\text{in,p}} \ddot{\mathbf{x}}^e - \mathbf{f}_{\text{in,p}}]. \quad (10)$$

Here, we have introduced the column vector of nodal coordinates of the element,

$$\mathbf{x}^e = \begin{bmatrix} \mathbf{x}^p \\ \boldsymbol{\vartheta}^p \\ \mathbf{x}^q \\ \boldsymbol{\vartheta}^q \end{bmatrix}, \quad (11)$$

the mass matrix

$$\mathbf{M}_{\text{in,p}} = \frac{\rho_p A_p l_0}{420} \begin{bmatrix} 156\mathbf{I} & 22l_0\mathbf{B}^p & 54\mathbf{I} & -13l_0\mathbf{B}^q \\ 22l_0\mathbf{B}^{pT} & 4l_0^2\mathbf{B}^{pT}\mathbf{B}^p & 13l_0\mathbf{B}^{pT} & -3l_0^2\mathbf{B}^{pT}\mathbf{B}^q \\ 54\mathbf{I} & 13l_0\mathbf{B}^p & 156\mathbf{I} & -22l_0\mathbf{B}^q \\ -13l_0\mathbf{B}^{qT} & -3l_0^2\mathbf{B}^{qT}\mathbf{B}^p & -22l_0\mathbf{B}^{qT} & 4l_0^2\mathbf{B}^{qT}\mathbf{B}^q \end{bmatrix} \quad (12)$$

and the convective terms

$$-\mathbf{f}_{\text{in,p}} = \frac{\rho_p A_p l_0}{420} \begin{bmatrix} 22l_0\dot{\mathbf{B}}^p\dot{\boldsymbol{\vartheta}}^p - 13l_0\dot{\mathbf{B}}^q\dot{\boldsymbol{\vartheta}}^q \\ 4l_0^2\mathbf{B}^{pT}\dot{\mathbf{B}}^p\dot{\boldsymbol{\vartheta}}^p - 3l_0^2\mathbf{B}^{pT}\dot{\mathbf{B}}^q\dot{\boldsymbol{\vartheta}}^q \\ 13l_0\dot{\mathbf{B}}^p\dot{\boldsymbol{\vartheta}}^p - 22l_0\dot{\mathbf{B}}^q\dot{\boldsymbol{\vartheta}}^q \\ -3l_0^2\mathbf{B}^{qT}\dot{\mathbf{B}}^p\dot{\boldsymbol{\vartheta}}^p + 4l_0^2\mathbf{B}^{qT}\dot{\mathbf{B}}^q\dot{\boldsymbol{\vartheta}}^q \end{bmatrix}, \quad (13)$$

where we have used the quantities

$$\mathbf{B}^p = \frac{\partial \mathbf{e}_x^p}{\partial \boldsymbol{\vartheta}^p}, \quad \mathbf{B}^q = \frac{\partial \mathbf{e}_x^q}{\partial \boldsymbol{\vartheta}^q}, \quad \dot{\mathbf{B}}^p = \frac{\partial \mathbf{B}^p}{\partial \boldsymbol{\vartheta}^p} \dot{\boldsymbol{\vartheta}}^p, \quad \dot{\mathbf{B}}^q = \frac{\partial \mathbf{B}^q}{\partial \boldsymbol{\vartheta}^q} \dot{\boldsymbol{\vartheta}}^q. \quad (14)$$

The velocity of the fluid at a stream line is directed along the axis of the pipe and can be approximated as

$$\mathbf{v}_f(\xi) = \dot{\mathbf{x}}(\xi) + v(\xi)\mathbf{x}'(\xi), \quad (15)$$

where the prime denotes a derivative with respect to s and v represents the relative velocity of the fluid with respect to the pipe. The velocity is scaled with the length of \mathbf{x}' , so a constant value of v does not represent a constant relative velocity for an extensible pipe; it conserves the mass of the fluid between two material cross-sections, however. The acceleration of the fluid is

$$\mathbf{a}_f(\xi) = \ddot{\mathbf{x}}(\xi) + [\dot{v}(\xi) + v(\xi)v'(\xi)]\mathbf{x}'(\xi) + 2v(\xi)\dot{\mathbf{x}}'(\xi) + [v(\xi)]^2\mathbf{x}''(\xi) \quad (16)$$

For an inextensible pipe, the terms on the right-hand side are easily identified as the entrainment acceleration of the pipe, the relative acceleration, the Coriolis acceleration and the centripetal acceleration. For steady flow, the second term disappears. The same interpolation is used as for the pipe, Eq. (9). The first term, the entrainment acceleration, gives a contribution to the virtual work having the same form as that due to the acceleration of the pipe, Eqs. (12) and (13), with the difference that $\rho_p A_p$ is replaced with $\rho_f A_f$, where ρ_f is the mass per unit of reference volume of the fluid, which is here equal to ρ_{f0} . For a non-uniform velocity distribution over the cross-section, the mass flow rate, \dot{m} , is the area times the average fluid velocity, as can be seen from

$$\dot{m} = \int v \rho_f dA_f = \rho_f A_f \bar{v}, \quad (17)$$

where \bar{v} is the average velocity. For the impulse flow rate, we have

$$\int \rho_f \|\mathbf{x}'\| v^2 dA_f = \rho_f A_f \|\mathbf{x}'\| \bar{v}^2 \approx \rho_f A_f k_v \bar{v}^2 = \frac{k_v \dot{m}^2}{\rho_f A_f}, \quad (18)$$

where $k_v > 1$ is a factor that measures the deviation from a uniform velocity distribution. For fully developed turbulent flow, this factor is a few percents larger than one, but for laminar flow in a pipe with circular cross-section, we have $k_v = 4/3$. The Coriolis acceleration gives a contribution to the virtual work of

$$-\frac{\dot{m}}{30} \delta \mathbf{x}^{eT} \begin{bmatrix} \mathbf{O} & 6l_0 \mathbf{B}^p & 30\mathbf{I} & -6l_0 \mathbf{B}^q \\ -6l_0 \mathbf{B}^{pT} & \mathbf{O} & 6l_0 \mathbf{B}^{pT} & -l_0^2 \mathbf{B}^{pT} \mathbf{B}^q \\ -30\mathbf{I} & -6l_0 \mathbf{B}^p & \mathbf{O} & 6l_0 \mathbf{B}^q \\ 6l_0 \mathbf{B}^{qT} & l_0^2 \mathbf{B}^{qT} \mathbf{B}^p & -6l_0 \mathbf{B}^{qT} & \mathbf{O} \end{bmatrix} \dot{\mathbf{x}}^e - \dot{m} \delta \mathbf{x}^{eT} \begin{bmatrix} -\dot{\mathbf{x}}^p \\ \mathbf{0} \\ \dot{\mathbf{x}}^q \\ \mathbf{0} \end{bmatrix}, \quad (19)$$

where \mathbf{O} and \mathbf{I} represent zero matrices and identity matrices of the appropriate dimensions and a part has been split off in order to make the gyroscopic matrix skew-symmetric. The centripetal acceleration yields a contribution to the virtual work of

$$-\frac{k_v \dot{m}^2}{30 l_0 \rho_f A_f} \delta \mathbf{x}^{eT} \begin{bmatrix} -36\mathbf{x}^p - 3l_0 \mathbf{e}_x^p + 36\mathbf{x}^q - 3l_0 \mathbf{e}_x^q \\ -3l_0 \mathbf{B}^{pT} \mathbf{x}^p - 4l_0^2 \mathbf{B}^{pT} \mathbf{e}_x^p + 3l_0 \mathbf{B}^{pT} \mathbf{x}^q + l_0^2 \mathbf{B}^{pT} \mathbf{e}_x^q \\ 36\mathbf{x}^p + 3l_0 \mathbf{e}_x^p - 36\mathbf{x}^q + 3l_0 \mathbf{e}_x^q \\ -3l_0 \mathbf{B}^{qT} \mathbf{x}^p + l_0^2 \mathbf{B}^{qT} \mathbf{e}_x^p + 3l_0 \mathbf{B}^{qT} \mathbf{x}^q - 4l_0^2 \mathbf{B}^{qT} \mathbf{e}_x^q \end{bmatrix} - \frac{k_v \dot{m}^2}{\rho_f A_f} \delta \mathbf{x}^{eT} \begin{bmatrix} -\mathbf{e}_x^p \\ \mathbf{0} \\ \mathbf{e}_x^q \\ \mathbf{0} \end{bmatrix}. \quad (20)$$

A part has been split off, so the remaining part yields a symmetric contribution to the stiffness matrix of the linearized equations.

The boundary conditions at the nodes need special attention. If the pipe joins smoothly to the next pipe and there are no jumps in the cross-section, no further terms are needed. Furthermore, the terms that have been split off in Eqs. (19) and (20) cancel for the two elements in the assembly of the system equations and need not be taken into account. If two pipes are joined at an angle, or if the cross-section changes, the contribution caused by the change in impulse of the fluid in the kink has to be taken into account. We propose to add a pair of forces at the element

from which the fluid emerges so that the fluid comes to rest with respect to the global inertial system and to add another pair of forces at the entrance of the next element which accelerates the fluid to the required speed. At the outlet, the decelerating force is

$$\mathbf{F}^q = -\dot{m}\dot{\mathbf{x}}^q - \frac{k_v \dot{m}^2}{\rho_f A_f} \mathbf{e}_x^q \quad (21)$$

and at the entrance of the next pipe element, the accelerating force is

$$\mathbf{F}^p = \dot{m}\dot{\mathbf{x}}^p + \frac{k_v \dot{m}^2}{\rho_f A_f} \mathbf{e}_x^p. \quad (22)$$

The same forces with opposite signs react on the pipe and these cancel with the split-off terms in Eqs. (19) and (20). If more than two pipes meet at a manifold, the same procedure can be used if the distribution of flow rates over the pipes is known. If a pipe sucks fluid from a large stationary reservoir, the boundary condition can be taken into account in the same way by introducing an additional force. For a free jet at the outlet of a pipe, no additional forces are needed.

2.3 Equations of motions

The pipe element is embedded in a multibody system dynamics program, SPACAR [12]. In this program, the equations of motion are formulated numerically in terms of independent generalized coordinates \mathbf{q} as

$$\mathbf{M}(\mathbf{q}, t)\ddot{\mathbf{q}} = \mathbf{Q}(\dot{\mathbf{q}}, \mathbf{q}, t), \quad (23)$$

where \mathbf{q} is the system mass matrix and \mathbf{Q} is the vector of generalized forces, including inertia terms. Moreover, the linearized equations for a given state can be formulated as

$$\mathbf{M}\Delta\ddot{\mathbf{q}} + \mathbf{C}\Delta\dot{\mathbf{q}} + \mathbf{K}\Delta\mathbf{q} = \mathbf{0}, \quad (24)$$

where \mathbf{C} and \mathbf{K} are the damping and stiffness matrices, respectively. The prefixed Δ denotes a small increment. More information on the linearization, also including input and output relations, can be found in [13].

3 EXAMPLES OF APPLICATION

3.1 Straight simply supported pipe

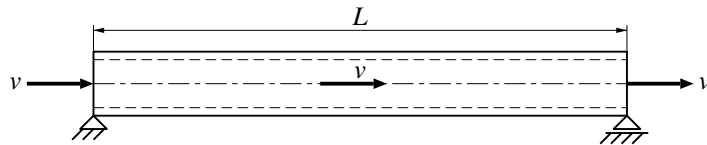


Figure 1: Simply supported pipe.

In a first test problem, we consider a straight pipe that is simply supported at its ends and supported in the axial direction at its inlet, see Fig. 1. The static buckling loads are the same as those of an Euler column with a compressive force of $k_v \dot{m}^2 / (\rho_f A_f)$, so the lowest critical mass-flow rate for a simply supported pipe of length L is $\dot{m}_{cr} = (\pi/L) \sqrt{\rho_f A_f EI / k_v}$. We consider the case with $EI = 1$, $L = 1$, $\rho_p A_p = 0.75$, $\rho_f A_f = 0.25$, $k_v = 1$ in arbitrary units. The pipe is subdivided into 1, 2, 4, 8 or 16 equal elements. Table 1 gives the values of the critical mass-flow rate. It can be seen that the order of convergence is 4.

number of elements	critical mass-flow rate	error
1	1.732050808	0.161254481
2	1.576693278	0.005896951
4	1.571198510	0.000402183
8	1.570822061	0.000025734
16	1.570797945	0.000001618
∞	1.570796327	

Table 1: Numerical critical mass-flow rates \dot{m}_{cr} for a simply supported pipe.

3.2 Straight cantilever pipe

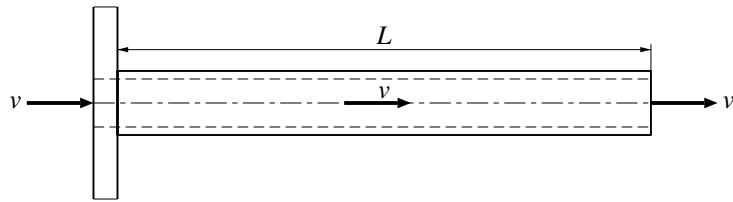


Figure 2: Cantilever pipe.

Next, an example given in [8] with a straight cantilever pipe is considered, see Fig. 2. The parameters for the pipe are $L = 1$ m, $EI = 10$ Nm², $\rho_p A_p = 8$ kg/m, $\rho_f A_f = 2$ kg/m, and $k_v = 1$. The critical mass-flow rate at which the trivial solution becomes unstable in a Hopf bifurcation (flutter), is given in Table 2 for discretizations with different numbers of equal elements. The critical flow velocities can be readily found from these values by dividing them by the mass per unit of length of the fluid. Exact solutions are not available for this case. In [8], a critical mass-flow rate of 25.202 kg/s is given. The order of convergence is again 4.

number of elements	critical mass-flow rate [kg/s]	difference [kg/s]
2	24.962732	
4	25.054732	-0.092000
8	25.008910	0.045822
16	25.005738	0.003172
32	25.005534	0.000204
extrapolated	25.005520	0.000014

Table 2: Numerical critical mass-flow rates \dot{m}_{cr} for a cantilever pipe.

In a second test, the same pipe is deflected by a lateral tip force of 1.5 N, which results in a static deflection of about 0.05 m if no flow is present. The transient tip deflection if a mass-flow rate of 30 kg/s starts to flow is calculated. The motion approaches a limit cycle. The transverse deflection if the pipe is modelled with 2, 4 or 8 equal elements is shown in Fig. 3. Fewer elements than in [8] are needed to obtain a reasonable accuracy.

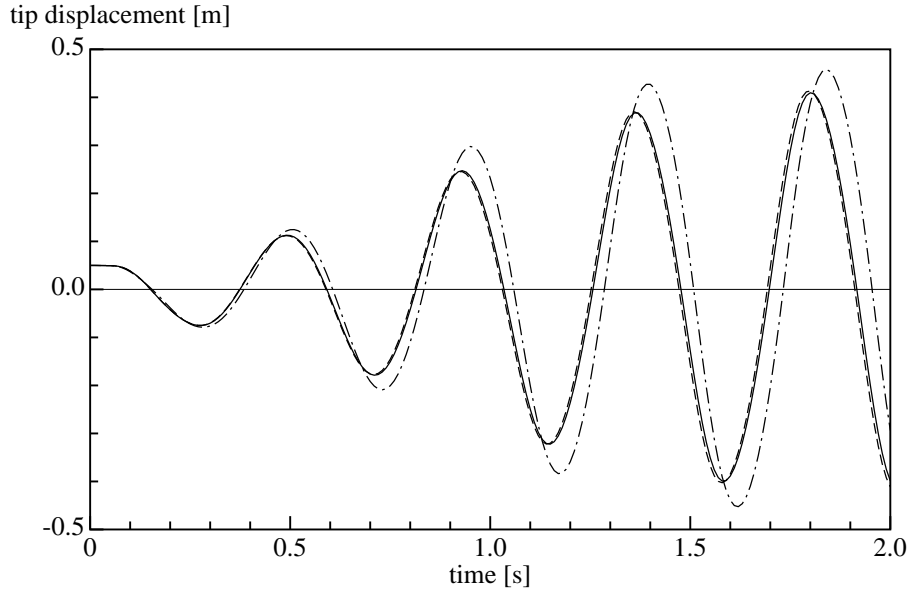


Figure 3: Transient tip deflection for a cantilever pipe with $\dot{m} = 30 \text{ kg/s}$; dashed-dotted: 2 elements; dashed: 4 elements; fully drawn: 8 elements.

3.3 Semicircular rotating pipe

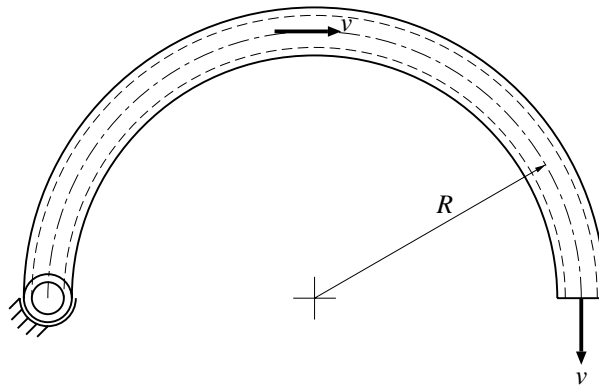


Figure 4: Semicircular rotating pipe.

A semicircular pipe that can rotate about an axis perpendicular to its plane at its inlet is shown in Fig. 4. Owing to the fluid flow, the pipe starts to rotate until a stationary angular velocity is reached, as happens in a garden sprinkler. The parameters for the pipe are chosen the same as in [8]: $R = 0.5 \text{ m}$, $\rho_p A_p = 0.5 \text{ kg/m}$, $\rho_f A_f = 1 \text{ kg/m}$, $k_v = 1$ and $\dot{m} = 10 \text{ kg/s}$. Different flexural rigidities are considered: $EI = 10 \text{ Nm}^2$, $EI = 100 \text{ Nm}^2$ and $EI = 1000 \text{ Nm}^2$. Also a rigid pipe is analysed as a reference. The motion is started from the undeformed configuration with zero initial velocities. The semicircular pipe is modelled by eight equal, curved elements. Fig. 5 shows the resulting angular velocity at the inlet over the first second for the four different flexural rigidities. The final angular velocities are 5.218466 rad/s for $EI = 10 \text{ Nm}^2$, 9.009825 rad/s for $EI = 100 \text{ Nm}^2$, 9.882486 rad/s for $EI = 1000 \text{ Nm}^2$, and 10.0 rad/s for a rigid pipe. The final angular velocities are smaller for the flexible pipes than for a rigid pipe, because a flexible

pipe straightens under influence of the fluid flow.

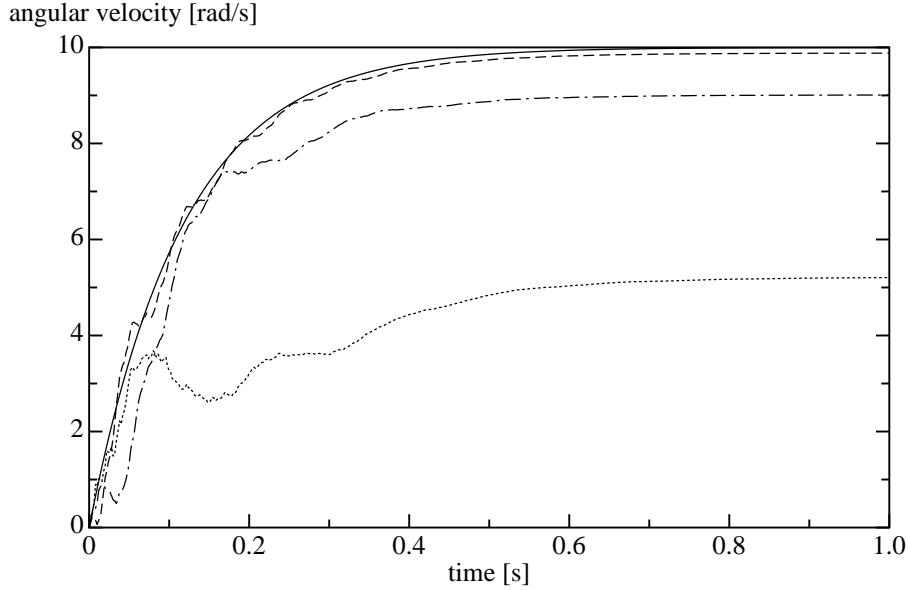


Figure 5: Angular velocity of a rotating curved pipe; dotted: $EI = 10 \text{ Nm}^2$; dashed-dotted: $EI = 100 \text{ Nm}^2$; dashed: $EI = 1000 \text{ Nm}^2$; fully drawn: rigid.

It is interesting to see what happens if the pipe is submersed in a large reservoir and fluid is sucked out through the curved pipe. An anecdote about an experiment on this problem was related by Feynman [15], which resulted in a burst carboy, but no results were revealed. The result from our simulation is that almost no motion occurs. This was confirmed by Païdoussis [16, 1].

4 CORIOLIS MASS-FLOW RATE METER

The previous test problems are all two-dimensional. As a three-dimensional problem, a Coriolis mass-flow rate meter is considered, which consists of a pipe in a plane configuration which mainly executes vibrations out of its plane.

Before a specific example is analysed, some general observations on these meters are made. The main part of the meter is a pipe with uniform cross-section whose centre line forms some curve in space and whose ends, the inlet and the outlet, are firmly fixed. The principle on which the instrument operates is that an eigenmode is excited and the change in the mode shape due to the fluid flow is observed. Only the case of a constant mass-flow rate will be considered. The acceleration of the fluid can be expressed as in Eq. (16) with the second term equal to zero. The virtual work of the centripetal term can be transformed as

$$-\int_0^L \rho_f v^2 \delta \mathbf{x}^T \mathbf{x}'' ds = -[\rho_f v^2 \delta \mathbf{x}^T \mathbf{x}']_0^L + \int_0^L \frac{1}{2} \rho_f v^2 \delta [(\mathbf{x}')^T \mathbf{x}'] ds. \quad (25)$$

The first term on the right vanishes, because the ends are held fixed and the second term vanishes if the pipe is assumed to be inextensible. This means that the centripetal acceleration is provided by the normal force in the pipe. An exception is a straight pipe, where the normal force is indeterminate, which is not considered here any further. From this we can conclude that no static instability can be caused by the fluid flow, as the time-independent term in the virtual

work related to the fluid flow has been eliminated. For slender pipes, with relatively high normal stiffness, the centripetal acceleration is still mainly supplied by the normal force and static instability can be expected only at very large mass-flow rates. The Coriolis acceleration does not yield any net energy input or dissipation and gives rise to a skew-symmetric gyroscopic matrix C in the linearized equations of motion. Because the total mechanical energy remains constant if all material and external damping is neglected, no flutter instability can occur. The eigenfrequencies for the linearized equations of motion are all real, but the modes are complex because of the gyroscopic matrix, which means that for a particular mode, the motion of different parts of the pipe have phase differences. In the limit for large mass-flow rates, the gyroscopic terms tend to dominate in the fluid acceleration and the eigenfrequencies approach zero as $1/v$. Indeed, a flexible string that moves axially at a high speed, as can occur in belt drives, has the tendency to maintain any spatial curve it is forced into [14, p. 608].

Normally, mass-flow rate meters operate at low flow rates and the previous considerations are of minor importance. The fluid flow can be considered as a small perturbation on the case of zero flow rate. As the Coriolis acceleration is 90° out of phase with the displacement, there is no first-order influence on the natural frequencies. If the pipe is excited in a particular mode of the system without fluid flow, the Coriolis acceleration can be seen as an excitation term for the other modes of the system.

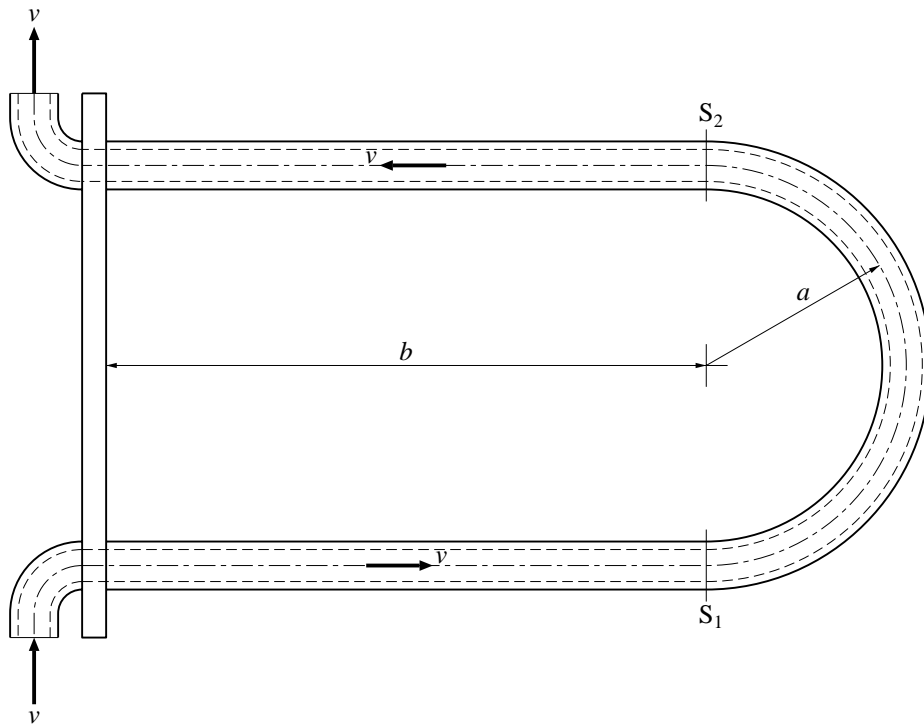


Figure 6: U-shaped mass-flow rate meter pipe. The sensors are at the positions S_1 and S_2 .

The example of a U-shaped pipe as in [9] is considered, see Fig. 6. The pipe consists of a semicircular part with radius a and two straight legs of length b , which are connected to the fixed world. The pipes have an outer diameter of 50.8 mm and an inner diameter of 47.2 mm and are made of steel with $E = 208$ GPa, $G = 80$ GPa, $\rho_p = 8027$ kg/m³, and $a = 150$ mm, whereas b can be given several values. The fluid is water with $\rho_f = 1000$ kg/m³ or kerosene

with $\rho_f = 780 \text{ kg/m}^3$. The finite element model uses two equal pipe elements for each leg and twelve equal, curved pipe elements for the semicircular arc.

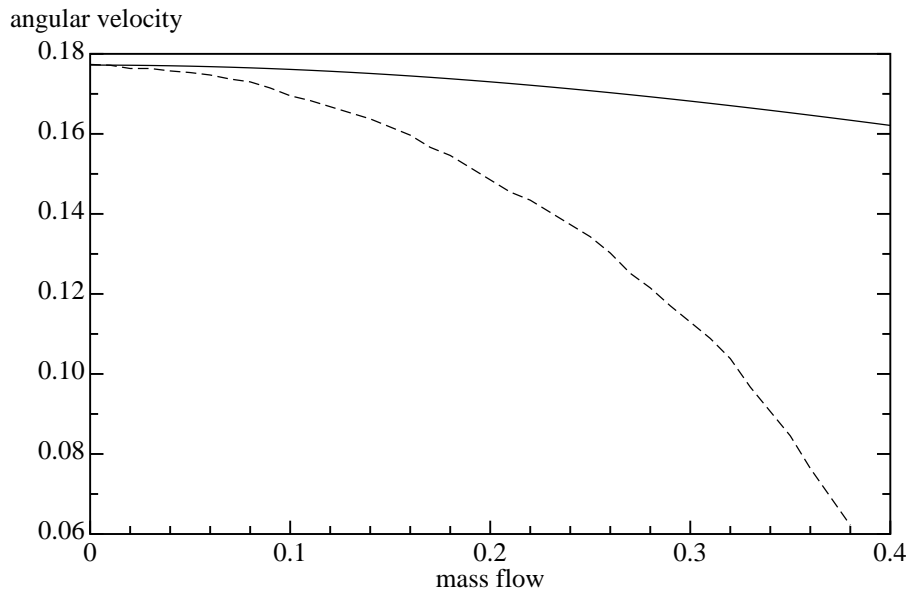


Figure 7: Dimensionless natural frequency as a function of the dimensionless mass-flow rate for a water-filled pipe with $b = 3a$; fully drawn: present study; dashed: from [9].

Figure 7 shows the non-dimensionalized first natural frequency as a function of the non-dimensionalized mass-flow rate for a pipe filled with water for $b = 3a$. The corresponding mode shape consists mainly of a swinging of the pipe along an axis perpendicular to the legs, with a small twist motion along an axis parallel to the legs superimposed on it. The natural circular frequencies are scaled with $\omega_0 = \sqrt{EI/(\rho_p A_p + \rho_f A_f)}/a^2$ and the mass-flow rate is scaled with $\dot{m}_0 = \sqrt{\rho_f A_f EI}/a$. It can be seen that the reduction of the natural frequency is much less than was predicted in [9, Figure 9], where the influence of the normal force was neglected.

Figure 8 shows the time difference between the zero crossings at the two ends of the semicircular arc as a function of the scaled mass-flow rate for the case $b = 495 \text{ mm}$ and water or kerosene as the fluid. It is seen that the time difference depends mainly on the mass-flow rate and is very nearly independent of the density of the fluid. The almost perfectly straight line agrees well with the theoretical and experimental results in [9]. The neglected influence of the normal force in the equations there has almost no influence, since the dimensionless mass-flow rate is so small. The results for the eigenfrequencies and the sensitivities were confirmed by an independently developed program.

5 CONCLUSIONS

A finite pipe element has been developed that can be used to model flexible pipes conveying fluid that can undergo large additional rigid-body displacements. The test examples show that the developed element performs well in planar problems.

The application to a Coriolis mass-flow rate meter shows that spatial problems can be handled as well. The influence of the normal force in the pipe caused by the flow has been properly

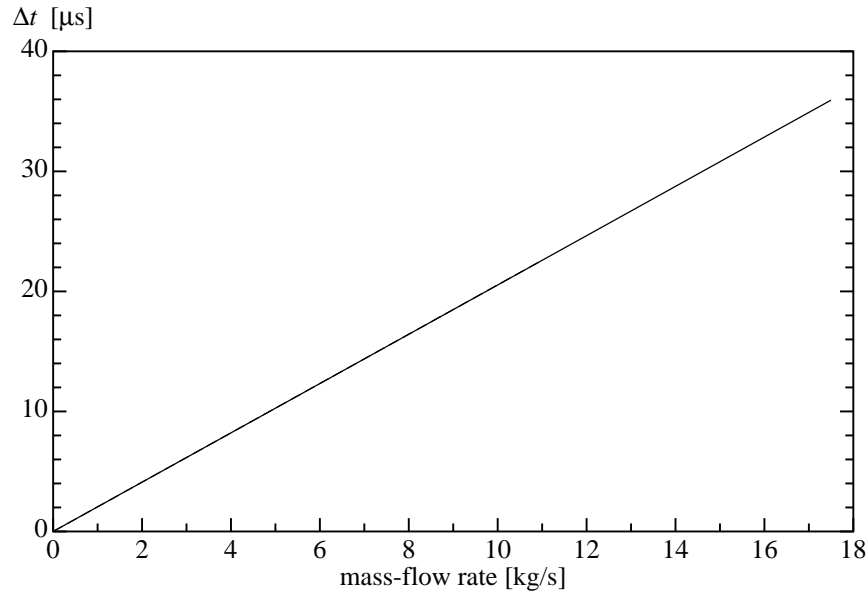


Figure 8: Time difference of zero crossing between the two measurement points as a function of the mass-flow rate.

included in the model, an effect that has often been neglected in previous analyses. No instabilities occur for realistic mass-flow rates.

REFERENCES

- [1] M.P. Paidoussis, *Fluid–structure interactions: slender structures and axial flow*, Vol. 1. Elsevier Academic Press, Oxford, 1998.
- [2] T.B. Benjamin, Dynamics of a system of articulated pipes conveying fluid I. Theory. *Proceedings of the Royal Society of London A*, **261**, 457–486, 1961.
- [3] T.B. Benjamin, Dynamics of a system of articulated pipes conveying fluid II. Experiments. *Proceedings of the Royal Society of London A*, **261**, 487–499, 1961.
- [4] H. Irschik and H.J. Holl, The equations of Lagrange written for a non-material volume. *Acta Mechanica*, **153**, 231–248, 2002.
- [5] R.W. Gregory and M.P. Paidoussis, Unstable oscillation of tubular cantilevers conveying fluid I. Theory. *Proceedings of the Royal Society of London A*, **293**, 512–527, 1966.
- [6] R.W. Gregory and M.P. Paidoussis, Unstable oscillation of tubular cantilevers conveying fluid II. Experiments. *Proceedings of the Royal Society of London A*, **293**, 528–542, 1966.
- [7] A.K. Bajaj and P.R. Sethna, Flow induced bifurcations to three-dimensional oscillatory motions in continuous tubes. *SIAM Journal on Applied Mathematics*, **44**, 270–286, 1984.
- [8] M. Stangl, J. Gerstmayr and H. Irschik, A large deformation planar finite element for pipes conveying fluid based on the absolute nodal coordinate formulation. *Journal of Computational and Nonlinear Dynamics*, **4**, 031009-1–8, 2009.

- [9] G. Sultan and J. Hemp, Modelling of the Coriolis mass flowmeter. *Journal of Sound and Vibration* **132**, 473–489, 1989.
- [10] A. Mehendale, *Coriolis mass flow rate meters for low flows* (doctoral dissertation). University of Twente, Enschede, 2008.
- [11] J.P. Meijaard, Validation of flexible beam elements in dynamics programs. *Nonlinear Dynamics* **9**, 21–36, 1996.
- [12] J.B. Jonker and J.P. Meijaard, SPACAR—computer program for dynamic analysis of flexible spatial mechanisms and manipulators. W. Schiehlen (ed.), *Multibody Systems Handbook*, Springer-Verlag, Heidelberg, 123–143, 1990.
- [13] J.B. Jonker, R.G.K.M. Aarts and J. van Dijk, A linearized input–output representation of flexible multibody systems for control synthesis. *Multibody System Dynamics*, **21**, 99–122, 2009.
- [14] G. Hamel, *Theoretische Mechanik, eine einheitliche Einführung in die gesamte Mechanik*. Springer-Verlag, Berlin, 1949.
- [15] R.P. Feynman, “*Surely you’re joking, Mr. Feynman!*” *Adventures of a curious character*. W.W. Norton and Company, New York/London, 1985.
- [16] M.P. Païdoussis, Fluid-structure interactions between axial flows and slender structures. T. Tatsumi, E. Watanabe and T. Kambe (eds.), *Theoretical and Applied Mechanics 1996* (Proceedings of the XIXth International Congress of Theoretical and Applied Mechanics, Kyoto, Japan, 25–31 August 1996), Elsevier, Amsterdam, 427–442, 1997.